applied optics

Predictive models for the Strehl ratio of diamond-machined optics

Hamidreza Aryan,[1,*] Kevin Liang,[2] Miguel A. Alonso,[2,3] and Thomas J. Suleski[1]

[1]Department of Physics and Optical Science, University of North Carolina at Charlotte, Charlotte, North Carolina 28223, USA
[2]The Institute of Optics, University of Rochester, Rochester, New York 14627, USA
[3]Aix Marseille Univ., CNRS, Centrale Marseille, Institut Fresnel, UMR 7249, 13013 Marseille, France
*Corresponding author: haryan@uncc.edu

Received 16 November 2018; revised 7 March 2019; accepted 26 March 2019; posted 26 March 2019 (Doc. ID 352179); published 19 April 2019

This paper provides a practical connection between the Strehl ratio as an optical performance metric and manufacturing parameters for diamond-machined optics. The choice of fabrication parameters impacts residual mid-spatial frequency groove structures over the part's surface, which reduce optical performance. Connections between the Strehl ratio and the fabrication parameters are studied using rigorous Rayleigh–Sommerfeld simulations for a sample optical system. The connections are generalized by incorporating the shape of diamond-machined groove structures and the effects of optical path differences for both transmissive and reflective optics. This work validates the analytical representation of the Strehl ratio as a Fourier transform of a probability density that relates to surface errors. The result is a practical tool that can be used to guide the choice of machining parameters to achieve a targeted optical performance.

https://doi.org/10.1364/AO.58.003272

1. INTRODUCTION

The development of computer-controlled sub-aperture fabrication techniques has opened new perspectives to the future of optics as well as new challenges [1,2]. Aspheric and freeform surfaces fabricated with such deterministic turning, milling, grinding, and polishing methods leave structured mid-spatial frequency (MSF) surface errors with "signatures" that can be identified with the specific fabrication processes [3,4]. Studies show that MSF errors can cause image artifacts and otherwise degrade optical performance [5–8]. In this paper, we address surface errors resulting from diamond machining processes, which appear primarily as cusp-shaped grating-like patterns, as shown in Fig. 1.

The specification of MSF errors on optical surfaces is sometimes overlooked by optical designers. This is partially due to limitations of commonly used surface specs for these types of errors [9], and partially because the impacts of MSF errors on optical performance are often underestimated or not well understood. Such errors can cause confusion between designers and manufacturers when a part does not perform as expected, even though it meets the requested surface specifications [10]. Therefore, to avoid poor performance, optical surfaces are often over-specified, which unnecessarily adds to manufacturing cycle times and costs. This motivates the present work, which uses a semi-empirical approach to connect the Strehl ratio (SR) directly to fabrication parameters for well-structured MSF errors from diamond machining processes.

A recent theoretical approach [11,12] expressed the SR and the optical transfer function (OTF) in terms of the Fourier transform of a probability density that is related to the statistics of the MSF structures. For the cases of diamond turned or milled surfaces, the circular cusps typically left behind are approximated as parabolic segments in order to attain an analytic expression for the SR, which can be written as

$$\mathrm{SR} = \frac{\pi}{4\phi}\left|\mathrm{erf}\left|(1+i)\sqrt{\frac{\phi}{2}}\right|\right|^2. \tag{1}$$

Here ϕ is the maximum optical phase difference resulting from the groove structures, and erf is the error function. This analytic expression is useful for further theoretical analysis; the goal in these prior works was to provide intuition on the behavior of the SR. In contrast, in this paper we provide prescriptive rules of thumb for optical manufacturers to optimize fabrication parameters based on SR. The semi-empirical approach proposed here also demonstrates a useful method to establish connections for additional surface error types that are difficult to describe analytically, providing a baseline for further work in this area. We now discuss a semi-empirical approach for connecting the SR to fabrication parameters for diamond-machined optics.

2. MODEL AND APPROACH

As a first step toward understanding behavioral changes in the SR with respect to fabrication parameters, we solve the problem for a case-specific situation. We developed a MATLAB toolbox

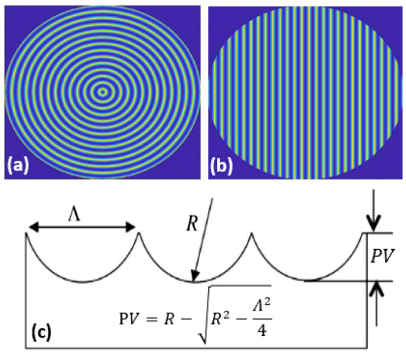

Fig. 1. Primary MSF residuals resulting from (a) diamond turning, (b) diamond raster milling, (c) cross section of the assumed MSF residuals. Λ represents the spacing between groove structures, R is the radius of the diamond tool tip, and PV is the peak-to-valley of the residual surface structure.

with three main operations: (1) synthesizing a lens model with desired form; (2) synthesizing a MSF texture (from either turning or milling) based on the input fabrication parameters and adding it to the surface of the lens; and (3) calculating the point spread function (PSF), OTF, and the SR of the resulting composite structure using rigorous Rayleigh–Sommerfeld simulations (RSS). The SR is defined as [13]

$$\mathrm{SR} \equiv \frac{\iint \mathrm{OTF}(f_x, f_y)\mathrm{d}f_x\mathrm{d}f_y}{\iint \mathrm{OTF}_{\mathrm{perfect}}(f_x, f_y)\mathrm{d}f_x\mathrm{d}f_y}. \tag{2}$$

Toolbox calculations were tested and compared to Rayleigh–Sommerfeld-based simulations within VirtualLab with excellent agreement. Standardized results are obtained by evaluating the performance of a diffraction-limited optic (prior to adding MSF errors) located at the aperture stop, similar to performance evaluation assumptions within Zygo's Mx software.

This toolbox enables us to assess changes in optical performance with respect to fabrication parameters. Our goal is to find general connections for reflective or transmissive optics for any wavelength or material without the need for more rigorous simulations. To this end, we first explore a specific case and then generalize the results.

In the case study, we assume a 4 mm diameter $f/25$ PMMA ($n = 1.4934$) lens at the pupil with plane wave illumination at $\lambda = 532$ nm. The diamond tool's tip radius, R, is set to 1 mm in this example. The machining feed per revolution (for diamond turning) or step-over (for diamond raster milling), collectively represented as Λ, is kept variable. A pixel size of $\delta x = 0.3$ μm was used for the RSS to enable SR values accurate to three decimal points. Figure 2 compares the simulation results of the SR versus Λ for both diamond-milled and diamond-turned surfaces. As we will discuss later in the paper, the differences between the performance of diamond-milled and diamond-turned surfaces are not reflected in SR simulations.

From a manufacturing perspective, increasing Λ is desirable as doing so reduces the required manufacturing time and cost. However, as expected, Fig. 2 shows that increasing Λ leads to a lower SR. In practice, Λ is normally chosen to be small enough

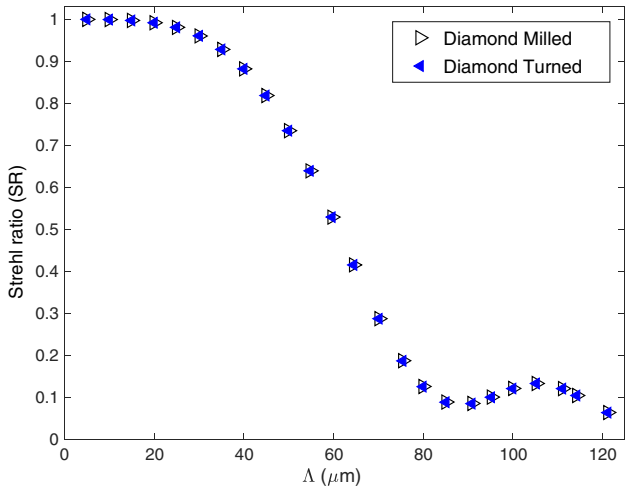

Fig. 2. Impact of diamond-machined MSF errors on the SR with respect to groove spacing for the specific case study. Simulation results indicate similar SR values for diamond-milled and diamond-turned optics (RMSE = 0.000172).

to meet a required root mean square (RMS) surface deviation that guarantees the smooth surface requirements.

We now generalize our results. Surface imperfections create wavefront distortions since an unwanted surface height leads to an undesired optical phase difference. An optical path difference of one wavelength, λ, results in a phase difference of 2π. Therefore, for a surface height of $h(x, y)$, the optical phase difference $\phi(x, y)$ equals

$$\phi(x, y) = kAh(x, y), \tag{3}$$

where $k = 2\pi/\lambda$, $A = n_s - n_0$ (in transmission) or $2n_0$ (in reflection), with n_s being the refractive index of a transmissive material, and n_0 the ambient refractive index.

For diamond-machined surfaces, it is straightforward to determine the relationship between the peak-to-valley (PV) of the residuals and the machining parameters:

$$PV = R - \sqrt{R^2 - \frac{\Lambda^2}{4}} = R - R\left[1 - \frac{\Lambda^2}{8R^2} + \frac{\Lambda^4}{128R^4} - \ldots\right] \approx \frac{\Lambda^2}{8R}, \tag{4}$$

where the approximation using the Taylor series expansion is valid for $R \gg \Lambda$. It is obvious that an increase in groove spacing results in a surface error with larger PV, which imparts a larger optical phase difference on the incident wavefront and lowers the SR, as seen in Fig. 2. By substituting PV in Eq. (4), for $h = \mathrm{PV}/\cos\theta_i$ in Eq. (3), where θ_i is the incident angle, we calculate the maximum optical phase difference imparted on the wavefront to be

$$\phi = \frac{kA}{\cos\theta_i}\left(R - \sqrt{R^2 - \frac{\Lambda^2}{4}}\right) \approx \frac{kA\Lambda^2}{8R\cos\theta_i}. \tag{5}$$

Equation (5), although conceptually intuitive, is an important outcome that enables a connection between the manufacturing parameters and optical performance. We note that the coordinate-dependent height function, $h(x, y)$, has been replaced with a

constant PV. This is justified since the diamond cusp surface shape is implicitly contained within the optical performance simulations shown in Fig. 2.

Next, we substitute the application parameters used in the case-specific example of Fig. 2 into Eq. (5), with no approximation, and perform a Gaussian fit [14] over the new dataset to obtain Eq. (6), which gives a general relation between the SR and ϕ for diamond-machined surfaces:

$$\mathrm{SR} \approx \exp\left[-\left(\frac{\phi}{3.24}\right)^2\right]. \tag{6}$$

We note from Fig. 3 that the fit is excellent for $\phi < 4.7$ rad with a root mean square error (RMSE) of 0.0036. We assert that this limit is sufficient for practical purposes since larger errors correspond to rough surfaces which fail basic RMS surface requirements and SR < 0.125. However, higher-order polynomial fits can be performed for larger values of ϕ if required. Figure 3 shows the resulting plot of the SR versus ϕ.

To provide a predictive tool we must invert Eq. (6):

$$\phi \approx 3.24\sqrt{-\log_e(\mathrm{SR})}. \tag{7}$$

This expression presents ϕ as a function of SR. Equation (7) provides a useful predictive tool for designers to quantify required surface specifications and for manufacturers to guide the choice of machining parameters based on the target SR.

We now present three example applications of the semi-empirical models. We note that SR values are given to several decimal places only to enable comparison of the model results.

Example 1: Predicting the SR from machining parameters for a lens. Consider a 5 mm diameter $f/10$ focusing element made of germanium ($n = 4.0242$) for use at $\lambda = 4$ μm. The lens is diamond-turned with $\Lambda = 50$ μm and $R = 1.5$ mm. Table 1 compares the on-axis prediction with simulation results.

As you can see from Table 1, after simulating the performance ($\delta x = 0.3$ μm) and calculating the SR, $\Delta = |\mathrm{SR_{RSS}} - \mathrm{SR_{predicted}}|$ is negligible. Therefore, Eq. (6) predicts SR without the need for more rigorous simulations.

Example 2: Predicting the SR from machining parameters for a mirror. Assume a 3 mm diameter $f/15$ focusing mirror operating at $\lambda = 480$ nm. The mirror is diamond-milled with $\Lambda = 25$ μm and $R = 1$ mm. In Table 2, we compare the predicted SR with the Rayleigh–Sommerfeld simulated SR ($\delta x = 0.3$ μm) for three different field angles.

In Table 2, predicted results are in excellent agreement with more rigorous, time-consuming simulations for all field angles with negligible differences.

Example 3: Determination of machining parameters for a required SR value. Consider an 8 mm diameter $f/5$ diamond-turned PMMA ($n = 1.4883$) lens working at $\lambda = 650$ nm. Assuming a diamond tool with $R = 0.5$ mm, we would like to find the maximum groove spacing Λ that results in an optic with on-axis SR = 0.9. Solving Eq. (7) for SR = 0.9 gives the maximum permitted optical phase difference of $\phi = 1.05$ rad. Substituting this value into Eq. (5) predicts $\Lambda \approx 29.82$ μm. To facilitate the performance simulation of this optic within MATLAB, we slightly modify Λ to 29.85 μm to generate an integer number of cusp errors per aperture and reduce the simulation resolution from $\delta x = 0.3$ μm to $\delta x = 0.6$ μm to overcome computational challenges. PSF and SR simulations confirm the accuracy of the semi-empirical model with simulated SR = $0.899 \approx 0.9$. In practice, the groove spacing could be rounded downward slightly (for example, to 29 μm) to provide additional performance margin and to simplify manufacturing setup.

Table 1. Predicted SR Versus Simulated SR for Example 1

Λ (μm)	R (mm)	ϕ (rad)	$\mathrm{SR_{Predicted}}$	$\mathrm{SR_{RSS}}$	Δ
50	1.5	0.990	0.910	0.914	0.004

Table 2. Predicted SR Versus Simulated SR for Different Field Angles

θ_i (deg)	ϕ (rad)	$\mathrm{SR_{Predicted}}$	$\mathrm{SR_{RSS}}$	Δ
0	2.05	0.670	0.669	0.001
21	2.19	0.633	0.630	0.003
30	2.36	0.588	0.583	0.005

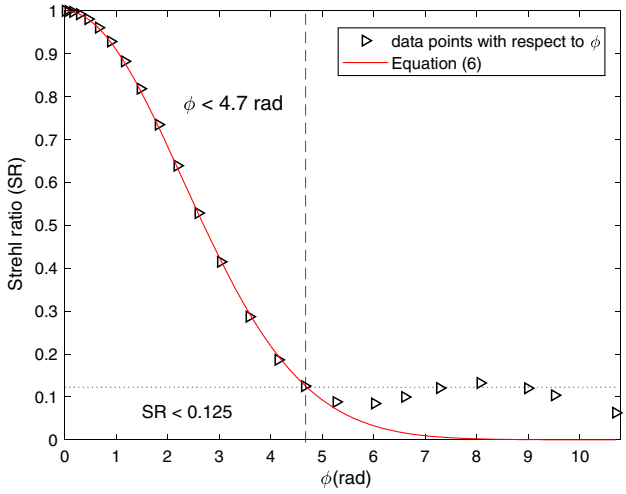

Fig. 3. SR versus optical phase difference (ϕ). The red curve represents Eq. (6).

3. DISCUSSION

The presented models can be used as tools to guide both the quantification of MSF surface specifications by optical designers and the choice of diamond machining parameters by manufacturers. As discussed previously, determination of the maximum groove spacing Λ for a given tool radius R that will still provide the required optical performance is desirable, as doing so reduces required manufacturing cycle time and cost.

For example, in diamond turning the groove spacing is determined by both the rotation rate of the machining spindle and the velocity (feed rate) of the diamond tool orthogonal to the axis of rotation. The resulting feed per revolution is then given by [4]

$$\Lambda = \frac{\mathrm{Feed(mm/min)}}{\mathrm{Spindle\ Speed(rev/min)}}. \tag{8}$$

Table 3 illustrates a range of representative manufacturing parameters for diamond turning the lens in Example 3

Table 3. Sample Manufacturing Parameters for Example 3

	SR	Λ_{Lens} (μm)	Λ_{Mirror} (μm)	R (mm)	Spindle (rpm)	$Feed_{Lens}$ (mm/min)	$Feed_{Mirror}$ (mm/min)
I	0.9	51	25	1.5	1500	76.5	37.5
II	0.9	47	23	1.25	1750	82.25	40.25
III	0.9	42	20	1	2000	84	40
IV	0.9	29	14	0.5	1000	29	14
V	0.9	29	14	0.5	2000	58	28

compared to a mirror with the same $f/\#$ and application parameters. The approximation in Eq. (5) helps to simplify these types of calculations. The differences in parameters for the lens and "equivalent" mirror result from the optical phase differences between the transmissive and reflective cases. Note that we have rounded the groove spacing down to the nearest integer value, which simplifies manufacturing setup and provides additional performance margin.

We note that there are other sources of MSF errors that occur in diamond-machined optical surfaces besides the "cusp" shapes that we have considered, including, for example, asynchronous error motions, external and self-induced vibration, thermal drift, materials effects, and so on [4,15–18]. These additional error sources are also connected to the feed rate and spindle speed. With the guidance of the presented models, a manufacturer can use their expertise to select the best combination of tool radius, feed rate, and spindle speed that gives the required result at minimal time and cost while also minimizing other sources of error.

The use and limitations of the SR as an optical performance metric for diamond-machined optics is worthy of additional consideration. Figure 2 suggests that the optical performance of diamond-turned and diamond-milled components with equivalent groove spacing Λ will be quite similar. While this is generally true for very high-quality optics, the performances of turned and milled components deviate as the groove spacing increases due to the difference in symmetry of the residual surface structures [10,12]. For such cases, other performance measurements, such as a 2D modulation transfer function, would represent optical performance more effectively than the SR. Such relationships and performance metrics are currently being studied and will be considered in more detail in future publications.

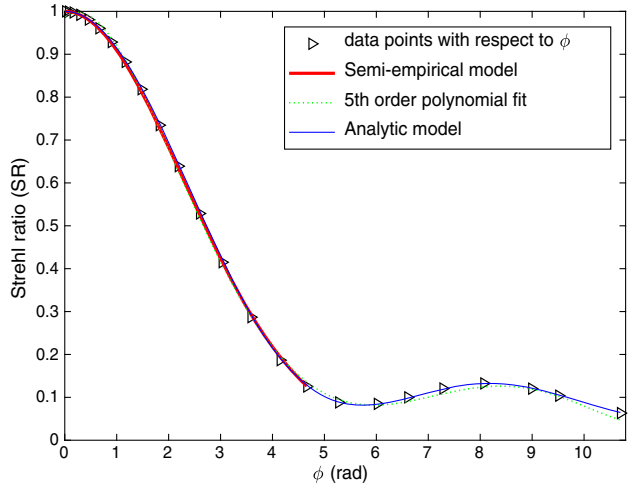

Fig. 4. Comparison of the semi-empirical and analytic SR expressions, given by Eqs. (6) and (1), respectively. For $\phi < 4.7$ rad, the two models differ by a RMSE of 0.0058.

Figure 4 compares the semi-empirical model of Eq. (6) with the analytic model of Eq. (1) and a fifth-order polynomial fit over the full range of ϕ values. This figure shows that the semi-empirical approach developed in this paper agrees very well with the analytic model based on prior work [11,12]. The close agreement supports the validity of both approaches. However, Eq. (6) is designed to be more succinct, user-friendly, and invertible to Eq. (7) to enable a predictive model for both manufacturer and designer, which is not the case with Eq. (1).

Funding. National Science Foundation (NSF) I/UCRC Center for Freeform Optics (IIP-1338877, IIP-1338898, IIP-1822026, IIP-1822049); Fondation Aix-Marseille Universite (Fondation AMU).

Acknowledgment. The authors would like to thank the members of CeFO for their support and insights and acknowledge useful discussions with Dr. Matthew Davies, Dr. Chris Evans, Dr. Angela Davies Allen, and Dr. Greg Forbes. M.A.A. acknowledges the Excellence Initiative of Aix-Marseille University - A*MIDEX, a French "Investissements d'Avenir" program.

REFERENCES

1. D. M. Aikens, J. E. DeGroote, and R. N. Youngworth, "Specification and control of mid-spatial frequency wavefront errors in optical systems," in *Frontiers in Optics 2008/Laser Science XXIV/Plasmonics and Metamaterials/Optical Fabrication and Testing*, OSA Technical Digest (CD) (Optical Society of America, 2008), paper OTuA1.
2. G. W. Forbes, "Never-ending struggles with mid-spatial frequencies," Proc. SPIE **9525**, 95251B (2015).
3. C. R. Dunn and D. D. Walker, "Pseudo-random tool paths for CNC sub-aperture polishing and other applications," Opt. Express **16**, 18942–18949 (2008).
4. M. Bass, C. DeCusatis, J. Enoch, V. Lakshminarayanan, G. Li, C. Macdonald, V. Mahajan, and E. V. Stryland, *Handbook of Optics*, 3rd ed. (McGraw-Hill, 2009), Volume **II**: Design, Fabrication and Testing, Sources and Detectors, Radiometry and Photometry, Chap. 10.
5. J. A. Shultz, M. Davies, and T. J. Suleski, "Effects of MSF errors on performance of freeform optics: Comparison of diamond turning and diamond milling," in *Imaging and Applied Optics*, OSA Technical Digest (online) (Optical Society of America, 2015), paper FT4B.3.
6. J. M. Tamkin, W. J. Dallas, and T. D. Milster, "Theory of point-spread function artifacts due to structured mid-spatial frequency surface errors," Appl. Opt. **49**, 4814–4824 (2010).
7. J. M. Tamkin, T. D. Milster, and W. J. Dallas, "Theory of modulation transfer function artifacts due to mid-spatial-frequency errors and its application to optical tolerancing," Appl. Opt. **49**, 4825–4835 (2010).
8. J. Filhaber, "Mid-spatial-frequency errors: the hidden culprit of poor optical performance," Laser Focus World **49**, 32 (2013).
9. Z. Hosseinimakarem, H. Aryan, A. Davies, and C. Evans, "Considering a Zernike polynomial representation for spatial frequency content of optical surfaces," in *Imaging and Applied Optics*, OSA Technical Digest (online) (Optical Society of America, 2015), paper FT2B.2.
10. H. Aryan, C. J. Evans, and T. J. Suleski, "On the use of ISO 10110-8 for specification of optical surfaces with mid-spatial frequency errors," in *Optical Design and Fabrication (Freeform, IODC, OFT)*, OSA Technical Digest (online) (Optical Society of America, 2017), paper OW4B.2.

11. M. A. Alonso and G. W. Forbes, "Strehl ratio as the Fourier transform of a probability density of error differences," Opt. Lett. **41**, 3735–3738 (2016).
12. K. Liang and M. A. Alonso, "Understanding the effects of groove structures on the MTF," Opt. Express **25**, 18827–18841 (2017).
13. J. W. Goodman, *Introduction to Fourier Optics* (Roberts & Company, 2005).
14. MathWorks, "*MATLAB Curve Fitting Toolbox: User's Guide (R2019a)*," (The MathWorks, 2019), Chapters 4 and 5.
15. S. Rakuff and P. Beaudet, "Thermally induced errors in diamond turning of optical structured surfaces," Opt. Eng. **46**, 103401 (2007).
16. K. Cheng, ed., *Machining Dynamics* (Springer, 2009), Chap. 9.
17. A. Sohn, L. Lamonds, and K. Garrard, "Modeling of vibration in single-point diamond turning," in *Proceedings of the Twenty-first Annual Meeting of the American Society of Precision Engineering (ASPE)* (2006), pp. 15–20.
18. J. A. Shultz, H. Aryan, J. D. Owen, M. A. Davies, and T. J. Suleski, "Impacts of sub-aperture manufacturing techniques on the performance of freeform optics," in *Proceedings ASPE/ASPEN Spring Topical Meeting: Manufacture and Metrology of Structured and Freeform Surfaces for Functional Applications* (2017), pp. 0061.